Applying a non-invasive multi-spectral sensing technique to two-phase flow measurements for pipeline monitoring

Zainal Abidin, D., Theminimulla, S., Waugh, D. G. & Griffin, J. M., Jun

Original citation & hyperlink: Zainal Abidin, D, Theminimulla, S, Waugh, DG & Griffin, JM 2022, 'Applying a non-invasive multi-spectral sensing technique to two-phase flow measurements for pipeline monitoring', International Journal of Energy and Environmental Engineering, vol. 13, no. 2, pp. 587-605. https://doi.org/10.1007/s40095-021-00471-4

DOI 10.1007/s40095-021-00471-4
ISSN 2251-6832
ESSN 2008-9163

Publisher: Springer

The final publication is available at Springer via http://dx.doi.org/10.1007/s40095-021-00471-4

Applying a Non-Invasive Multi-Spectral Sensing Technique to Two-phase Flow Measurements for Pipeline Monitoring

D. Zainal Abidin *, S. Theminimulla, D.G. Waugh, J.M. Griffin

School of Mechanical, Aerospace and Automotive Engineering, Faculty of Engineering, Environment and Computing, Coventry University, Gulson Road, Coventry, CV1 2JH, United Kingdom

*Corresponding Author:
D. Zainal Abidin
School of Mechanical, Aerospace and Automotive Engineering,
Faculty of Engineering, Environment and Computing,
Coventry University,
Gulson Road,
Coventry,
CV1 2JH, UK
Email: zainalad@uni.coventry.ac.uk / dzariff.zabidin@gmail.com

Abstract

"Smart" sensors, with a fusion-based approach, pave the way for potentially changing how pipeline network systems are controlled, maintained, and monitored. This is typically done through structural modeling or spot monitoring using micro-electromechanical systems (MEMS), strain gauges or through general conventional sensing. One of the challenges facing new developments in structural health monitoring (SHM) of a deployed asset is application to inaccessible locations. This work presents the use of a non-intrusive integrity monitoring sensor system utilising a multi-spectral approach to give more trusted insights to structural integrity as well as flow characteristics. The paper addresses the fundamental problems in identifying and characterising two-phase (air-water and oil-water) flow patterns and flow pattern transitions using numerous sensing techniques: strain gauges, optical Fibre Bragg Gratings (FBGs), thermocouples (K-type), accelerometers, acoustic emission analysis and gyroscopes. By providing low noise, un-biased strain measurements, the non-intrusive sensor system can verify and improve integrity monitoring, providing a reliable alternative to conventional sensing. In addition, the non-intrusive sensor system enables pressure monitoring, providing flow assurance data and, provides good data integrity, making it an ideal tool as an enhanced surveillance strategy in real time for SHM of pipeline networks.

Keywords: *acoustic emission signal, Fibre Bragg Grating (FBG) sensor, structural monitoring, sensor fusion, multiphase flow*

Introduction

Many studies around the world rely on extensive networks of pipelines to supply water, oil, and gas, extending over millions of miles, and with some pipeline networks running through harsh environment and terrains. Major pipeline failure incidents reported are caused mainly due to corrosion and leakage, causing significant damage to property [1-4]. Leakage issues are not only from wasting commodities, but also can cut profits and bring liability issues, directly affecting peoples' lives and the environment [5-9]. With this, it has become more noticeable in oil, water and gas industries where leaks can have major consequences and can last for many years. For example, the Trans Mountain pipeline leak in British Columbia gave rise to an estimated 195 barrels of crude oil being released in 2020 [10]. As a result of this and other incidents, the development of a non-intrusive sensor communication system for pipe SHM is crucial for pipeline networks [8]. Pipelines reaching the end of their lifespan, will result to failure by gradual leakage from erosion, abrasion, corrosion, and cracks. The pipelines are vulnerable to natural disasters, which may disrupt activity. Factors like this, risk a degradation for the pipeline performance. SHM sensing systems do exist for monitoring internal aspects of pipeline parameter which is to perceive flow rate, temperature, pressure, density, and viscosity which are structured as invasive techniques [11-16].

Multiple non-invasive SHM methods have been proposed, utilizing sensing devices that were placed or mounted on the exterior side of the wall pipes [7,9,17-23]. To detect pipe leakages, the approach of Zahab [9] uses acoustic emission (AE) sensing. That is, when leakages occur, the fluid would be released from the pipe wall producing acoustic activity. The acoustic information was obtained by placing acoustic emission sensors on the exterior of the pipe wall. From the collected data, the Author has used acoustic mapping of the pipe. This meant that leakages can be detected by analyzing the deviation from the baseline [17-19]. In [7], Santos showed that it is possible to detect small leakages using acoustic sensors placed at short distances between one another. However, it should be noted that background noise can negatively affect the sensitivity for large, turbulent flows. For another proposed technique, detecting leakages can be done through the installation of a long cable along the entire length of the pipe. With this, when the fluid is spilled, the liquid comes into contact with the installed cable causing a short circuit. This can only be applied for contact with conductive liquids such as water and hydrocarbon fluids [24,25]. Another variation, using a similar technique, is proposed by using optical fibres [13,20]. When there was a presence of a hydrocarbon leakage, the optical fiber measured the change in the refractive index. Another, a liquid sensing application method [21] is also based on using sensor cables. The principle involved is sending energy pulses along the cable, continuously and collecting the returned data samples. In the case of a leak, there would be a change in the impedance from the cable therefore obtaining a variation of echoes. Another type of sensing method is the application of vapor sensing, which is mostly used in tanks, less so in pipelines. Leakage detection is based on the use of analysis of concentration of the fluid vapor. The downfall to this application is the installation costs are very high and requires the deployment of many high value devices [20,22,23].

In the work done by Sharma [20], the Author has proposed a leakage detection system which is based on mass conservation. From fluid loss, a leakage would cause an inconsistency towards the flow i.e., upstream, and downstream from within the pipe. The method proposed measured changes in volume and mass from the pipeline entry and exit points. From a known pipeline diameter, the volume of fluid is said to be proportional to the velocity introduced pipe [21,26]. An ultrasonic method was applied for measuring the fluid velocity. By using this application, one of the advantages is that the technique is applicable non-intrusively. Transducers of this type can be mounted on the exterior of the pipe wall [27]. This characteristic is important as it would allow the system to be applied to an existing pipe system and enable flexibility towards the deployment.

Most, if not all, non-intrusive SHM sensor technologies utilize one technique. In order to increase resolution and accuracy, the work detailed within this manuscript shows how a multi-spectral approach can be taken. That is, strain gauges, optical fiber sensors Fibre Bragg Gratings (FBGs), thermocouples, accelerometers, and gyroscopes, in addition to acoustic emission have been employed to study the flow characteristics of a two-phase vertical pipe system, highlighting the advantages of using such a non-invasive multi-spectral approach. The objectives of the paper are therefore, to assess the correlation and physical link of flow through structural health of a pipe for two-phase flow measurement. Forming the construction and demonstration of a novel non-intrusive technique using sensor synergy and a multi-spectral approach. The significance of the technology could be readily applied to such industries as the oil and gas industry for pipeline health monitoring where difficult and remote access are essential for safety critical applications.

Set-up and Experimental Considerations

The pipe material was manufactured out of extruded Plexiglas, clear acrylic / Polymethyl-Methacrylate (PMMA) with an outer diameter of 90 mm, an inside diameter of 80 mm and a wall thickness of 5 mm. Standard telecommunication optical fibre Bragg gratings (FBGs) with central glass fibre core internal diameters of 125 µm, 250 µm external, including buffer acrylate coating and optical input interrogator, were used. The experimental set-up of the pipe, with the sensors, is shown in Figure 1 where the fibres are loaded circumferentially onto the pipe between two points at 1200 mm localised distance, overall good transfer of strain from enough tension through adhesive were applied to the fibre sensor. This distance is evaluated through series of experiments to measure the accuracy of gathered data fusion. The sensors were positioned circumferentially to prove that the internal pressure growth mimicked the discrete change of flow value; thus, there were differences between the signals recorded by reducing or increasing the flow. The values obtained can then be correlated to a Positive Displacement (PD) flow meter which measures the volumetric flow rate of fluids.

Electronic sensors (i.e., strain gauges, accelerometer, and gyroscope) were positioned near the FBG unit to compare respective configurations for resolution, overall sensitivity and compared against phenomena, crucial to be placed near the measurement point for all the signals to be synchronised. Due to the Bragg gratings act so that it measures both strain and temperature, one of the fibres was placed freely, not in contact with the pipe to measure the surrounding temperature. This will be the act of compensation; the thermocouple measured the temperature of the system. The visibility of the differences can be seen clearly to identify the strain, temperature, vibration, and acceleration from the flow. Three sets of tests were conducted to identify repeatability and to obtain mean averages of results.

The fibre interrogation tool communicated through WinACC software (Version 1.0.2.4). The data recorded was by unit measurement of absolute wavelength as a function of time and, in this case, related to strain and pressure from loading and freed fibre for temperature compensation. LabVIEW 2018 (Version 18, National Instruments) tool files were used for data for the combination of strain gauges (BF350+/-0.1Ω), Optical FBGs, thermocouple (K-type) OMEGA SA2F-KI-3M, accelerometer and gyroscope (3 Axis GY-521 MPU-6050). Input raw acquisition data within LabVIEW software was used to calculate strain and temperature from the FBGs, respectively. A MOOG Interrogator, NI-DAQ and Arduino microcontroller were implemented and synchronised into a single acquisition system. Flow was controlled progressively between 13 l/min– 26 l/min and the multiphase rig (Two-phase, liquid and air), which consisted of a control pump, flow meter and a combination of operating system i.e. the manual, electronic and flow-controlled valves, were controlled together within the multiphase flow system Omron CJ2M PLC and associated control equipment along with a Windows 10 desktop PC with EXOR's J-Mobile Runtime Software.

To further test the efficacy of the multi-spectral SHM technique, liquid (water/oil) that was released from the bottom of the pipe, shown in Figure 1, presented a controlled leak by manually and gradually loosening one of the pipe connections to represent a typical leakage. To produce the leakage scenario, the connection was loosened with the aperture size of approximately 5mm from the start of the leak and the pressure from within the pipe made the leak progressively worse and this can be seen within the results replicating the real-life situation and environment where the system had a connection that failed and showed what would happen in a catastrophic event. The flow rate within the pipe, before and after the leakage was recorded, the position of the leakage can be found in Figure 1 where the leakage is simulated. The significance of this leak is where the flow rate was measured from 18 l/min to 26 l/min respectively.

AE and Instrumentation Integration

Acoustic emission (AE) signals were recorded using an AEwin 1283 USB AE Node System (MISTRAS) and a built-in amplifying acquisition card. The sensors were connected to MISTRAS 1283 Acoustic Emission USB Node. Prior to use, the AE sensors were lubricated to ensure good interface contact from the emitting source propagating the signal of interest to the sensor, verifying the set-up from calibration i.e., pencil calibration [31] for the AE sensor. The sensor was mechanically clamped onto the external pipe using a specialised 3-D printed clamping system which was designed to house and clamp the sensor to a specific and static load.

An issue or problem raised during structural health monitoring is frequently distinguished with a sensor system that incorporates the use of several sensors that respond to the signature generated from independent phenomena [28]. Therefore, the developed suite of stand-alone sensors which when used together through synergy or additional insight from data fusion provide the advantage of additional information and confidence into a comprehensive evaluation for structural health monitoring as well as flow measurement. Using each sensor to its best advantage to meet the needs of specific application [29]. Both critical applications' accuracy and reliability can be increased by averaging their outputs, which allows for early damage and warnings and enables for necessary steps in reducing risks and damages that may pose [30].

Calibration Considerations

The Hsu-Nielson pencil break calibration method was carried out in accordance with worked provided by Hsu and Nielsen [31]. The calibration process was taken as a point of reference and was normalized from similar points. During the calibration, the average peak was recorded at 80 dB as seen in Figure 2(a) – (d). The calibration pencil lead breaking fracture was carried out five times and the average were taken. The sensors were synchronized to the data acquisition unit through signal conditioning and FBG interrogation linking the output to the user PC, through transfer mechanisms, interaction, and digital signal processing. Several auxiliary sensors were combined within one platform to allow online monitoring and data logging of the multiple electronic sensors and FBGs. The calibration of the sensors was conducted by determining the known value of flow rate conducted in the experiment to no flow and estimating sensor parameters such that the output will match to the known information.

The sensitivity of the FBG sensor was based upon an independent factor which induced strain in contact, leaving one sensor to act as temperature compensation. One FBG was placed unbonded, freely, as opposed to the sensor loaded to the pipe and was used to subtract the changes in the Bragg wavelength, the effective strain from the effect of temperature was compensated. Room and pipe temperature were taken into account during each test, subtracting the Bragg shift for the indication, unstrained and strained conditions. The FBG sensor was affected slightly by the change in temperature due to liquid temperature variation in the pipe over time. The calibration process was done by determining the known value of flow rate in the experiment and comparing it to a static flow and estimating such that the output matched with the known information.

Results and Discussion

Sensor Augmentation for Multiphase Flow Measurement

Flow rates were analysed based on the volumetric of water, oil, and air/liquid mixture. The comparison of the flow rates explained the physical change due to the introduction of different density and viscosity, increasing the percentage of oil being introduced in the pipe, increasing the ratio, correlating to the increased density and controlled rate, seeing the propagation and change to the increased ratio, equating to the sensor signals. Seeing the difference between the two phases and how they would behave and interact as oil is a slightly denser material than water, the transmission speed through oil was better. In the presence of water, FBG is submitted to a higher strain, and the strain difference causes the shifts in Bragg wavelength, which is the drop in signal amplitude.

As shown in Table 1, the anomaly from the top sensor of water and oil can be associated to a sudden increase in strain which can be explained by a shift in temperature changes. There is a high amplitude recorded, in Table 1, for both strain and acceleration which depicts that the pipe experienced the leakage. This is evidenced by comparing the bottom sensor and top sensor readings in Table 1. The accelerometer and gyroscope both detected a high amplitude signal from the shift, indicating that during this point the flow runs through the transition. There was an increase in wavelength change which highlighted the increased flow rate. The gradual linear increase of strain showed that the pressure increased linearly as the flow increased. This demonstrated that the sensor system can be used to readily identify real-time changes in flow and pressure through the change of strain in the pipe, detected by the wavelength shift of the FBG and strain sensors. When the system was subjected to a lower flow rate, the distance between the wavelength shifts dropped, in respect to pressure, giving a closer value in wavelength shift when comparing the bottom and top sensors. This demonstrated the importance of distance between the top and bottom sensors to detect wavelength shifts. This can also be seen when there was no flow and low pressure as the wavelength shift was broader and had increased. For a higher flow rate, the wavelength shift dropped drastically from 1550nm to 1549nm, and the difference between the wavelength shift of the bottom and top sensors was narrower compared to that of a low flow rate. It should also be noted that, whilst water and oil flow could be detected, the sensor signals were stronger for water when compared to oil. This was due to the fact that water is a denser liquid compared to oil. Furthermore, the denser liquid (water) gave rise to better transmission of signals. This is significant as it demonstrates that the multi-spectral SHM technique can be non-intrusively applied to detect flows of different liquids, with different densities. This could lead to the development of a system which can monitor liquid content within pipeline networks.

By comparison in Figure 3, strain is introduced lower in water than oil; the strain from the bottom pipe for oil showed more pronounced data as density depicted to these changes and can be seen clearly in comparison to water flow data. Excitation voltage seemed higher in water, resulting from a fluid temperature change between water and oil. The leakage phenomenon can be observed through the acceleration magnitude, pressure and strain when compared to water. Water recorded a much lower magnitude, strain value, and stable pressure at 13 cbar. The pipe has been shifted from its original position due to the leak and burst effect, which can be seen in the change towards angular velocity. Depicted that both scenarios were at a fixed flow rate of 13 l/min, this can mean that the data in oil produced the initial start of anomaly results.

The anomaly from the top sensor of water and oil can be associated with a sudden increase in a strain which can be explained by a shift in temperature changes. A high amplitude recorded for both strain and acceleration depicts that the pipe experienced leakage. This is evidenced by comparing the bottom sensor and top sensor readings. The accelerometer and gyroscope both detected a high amplitude signal from the shift, which justifies that vibrations were acting on the pipe. Indicating that the flow runs through the transition during this point. There was an increase in wavelength change which highlighted the increased flow rate. The gradual linear increase of strain showed that the pressure increased linearly as the flow increased.

This demonstrated that the sensor system could be used to readily identify real-time changes in flow and pressure through the change of strain in the pipe, detected by the wavelength shift of the FBG and strain sensors. When the system was subjected to a lower flow rate, the distance between the wavelength shifts dropped, with respect to pressure, giving a closer value in wavelength shift when comparing the bottom and top sensors. This demonstrated the importance of the distance between the top and bottom sensors to detect wavelength shifts. This can also be seen when there was no flow and low pressure as the wavelength shift was broader and had increased.

For a higher flow rate, the wavelength shift dropped drastically from 1550nm to 1549nm, and the difference between the bottom and top sensors' wavelength shift was narrower than that of a low flow rate. It should also be noted that, whilst water and oil flow could be detected, the sensor signals were stronger for water when compared to oil. This was because water is a denser liquid compared to oil. Furthermore, the denser liquid (water) gave rise to better transmission of signals. This is significant as it demonstrates that the multi-spectral SHM technique can be non-intrusively applied to detect flows of different liquids with different densities. This could lead to the development of a system that can monitor liquid content within pipeline networks.

The percentage of air was controlled to maintain its equivalent volumetric flow rate. In Table 2, from the increased flow rate, there was a correlation with increased strain due to higher pressure, following the inverse relationship between the pressure and speed at a point in a fluid. From this relationship, an increased flow rate, with higher pressure would give rise to a linear difference in the wavelength change showing that the circumferential strain on the pipe is more significant. As a result, the pipe strain can be determined knowing that the fluid velocity is proportional to the internal pressure growth. This highlights how this system can be utilised as a non-intrusive flow sensing device. Like the accelerometer, the displacement caused the change in capacitance which is measured and processed to a particular angular rate thus the sensor positioned at the bottom showed a high rise, depicted in Table 2 (accelerometer graph for both water and air). This multi-spectral approach enables efficient, non-intrusive flow sensing that can be validated using the multiple sensor technologies.

The FBG sensor was positioned to detect strain and measured an increase in wavelength (see Table 2) when flow was present. This also demonstrated how the system can be used as a flow sensor. A high amplitude signal from the wavelength shift indicated that, during this point, there was an increased flow rate. From the increased flow rate, there was an association to an increased strain. This proved that the method can be developed to form a flow sensor based on Bragg gratings and induced vibration from the flow, showing that the flow and strain is measured in the form of a signal/vibration. It should be noted that the data received from the FBG sensor, the accelerometer and the strain gauges correlated with one another, during flow operation, and can be used together to confidently predict flow characteristics.

Liquid/air observed a higher strain value for both the top and bottom sensor, which aligned to the excitation voltage recorded. Due to air and water pressure, the localised pressure and strain reading associated with the liquid/air mixture caused the high peak amplitudes. The bubble formation was picked up by the sensor passing through the bottom to the top sensor. The event is producing much more than the system is producing. Acceleration and angular velocity seemed higher in the liquid/air mixture due to the system's higher energy propagating into the pipe. There is a considerable pressure difference caused by the possible leak phenomenon in Figure 4. The angular velocity at this point can be seen comparable towards the reading for water flow at the same flow rate depicting the pipe experiencing a high shift from its original position, worsening the cause of failure towards the pipe as flow increased and fluid/air mixture introduced. The difference concerning strain and pressure is the corresponding increase towards the instrumentation.

Regarding time, AE picked up more noise at the bottom than at the top due to more pressure exerted at the pipe's bottom. When the bubbles are formed, the pressure increased at the bottom of the pipe. The increased pressure is due to bubble formation as it passes from the bottom to the top sensor (as seen from the random spikes in the whole signal duration). In work done by El-Alej [32], the Author signifies the sound waves generated could have resulted in amplitude spikes and correlated leakage phenomenon; therefore, it is assumed the spheroidal signal found throughout the duration is the representation of large bubbles formation, the amplitude of the spikes is part of the signal recorded as the bubbles formed along as it passes through respective sensors. Moreover, the signal recorded shifted from one sporadic event to another, depicting a delay of the bubble passing through the bottom sensor to the top sensor. This time interval can be categorised as the time duration for the bubbles to reach the top before the collapse.

Fluid density changed the limit to the amplitude range of the AE signal. The sensors obtained the correlation signals, amplifying the range from which it saturates after reaching a certain threshold. The high voltage peak amplitude recorded were mainly related to leakage as the fluid in the pipe, material, and elastic event compressing. The system's vibration was compared to the signals recorded in AE, and the change in amplitude for AE is the result of the material and elastic events compressing along with the fluid association. The transducers were compressing and tensile acting, which is related to the change in density, temperature, and system interface.

The peak that was recorded in AE was significant in every signal at different time intervals and amplitudes as opposed to noise from the system. The events that happened in the pipe was much more pronounced. The strain value matched the overall change in the flow due to local pressurisation inside the pipe, resulting in AE achieving large spikes. The random spikes found in AE data are the anomaly from within the disturbance that occurred in the pipe during recording. Multiple sensor data comparisons have been made and justified through the events that cause the disturbances, raising the spike in pressure, especially causing AE to change overall. When the leak occurred (from the noise factor/hits) over the pass filter, the noise noticed an event occurrence.

The event was not entirely systematic due to leakage; it happened as a one-off event. The scenario from when the leak occurred resulted in a large 4 V in general, making that an anomaly event during that time. A disturbance or external influence caused the irregular events in the pipe; thus, monitoring individual events inside the pipe from a multi-spectral perspective can be an inexpensive method to solve the related and said problems such as leaks could be identified before the event worsen. The accelerometer recorded massive change from vibration caused by local instability associated with when the leak occurred from when the leak occurred. The noise events recorded caused a noticeable change in the amplitude.

The rise time from the continuous signals instead of district peak waveform loss energy from the overall top sensor to the bottom sensor. Higher events from the bottom sensors were recorded due to leak occurrence. AE reaching high amplitude is the result of activity recorded by the bottom pipe from strain and vibration induced. This is also caused by the moving transition to a specific flow rate. An event of disturbance or noise, assuming the pipe moved (recorded by the angular velocity towards leak occurrence) were distinguishable because the baseline of pressure factor in respect to noise recorded was equal to that of the multi-phase rig; therefore, any events outside the noise boundary were considered an event happening.

Differences from increased flow resulted in a high gain value of change in amplitude. Seeing the difference in peak values between the tests conducted, both the AE sensor and electronic sensors showed the correlation when AE recorded high peak amplitudes. Progressing towards a higher flow rate, a change in vibration was noticeable. Through the increased flow, there can be seen not to pose much volumetric flow increment, but the sensors were able to distinguish the signals recorded, making the technique applicable to low flow rates.

Acoustic Emission (AE): Signals and their relation towards flow conditions

In association to the sensor responses, AE analyses sound generation along the pipeline and pinpointing the location, measuring the intensity of the noise source. When looking at crossing the pipe wall, the AE signal was subjected to noise effects, attenuation, reflection, and refraction. These effects made the acoustic wave differ from the original stimulated source. The two sensor points had a different propagation impacts of acoustic energy wave, which was dependent on the system configuration and physical properties of the medium. The waveform passed from the bottom to the top sensor with a time difference that can be used to give a waveform time of flight as depicted in the calibration process, as demonstrated by Shuib [37]. The experimental results showed that fluid flowed into the pipe at different rates and produced different acoustic pressure magnitudes and frequencies. The fluids used in this study were two-phase flow pattern (liquid-air). The peak time signal indicated the type of fluid and its magnitude indicates the flow rate [24,25]. As shown in Figures 5 A-D, the acoustic fingerprint of interest is distinct for different fluids. It was found that there was correlation between the acoustic pressures and the flow rate of both fluids for water and oil. Acoustic pressure increased with the flow rate and at different density. The main goal was to investigate the relationship between acoustic signals and its flow conditions in a vertical well [24,25,40,41]. For each experiment, sound peaks as a function of the fluid flow rate were recorded. Elastic waves obtained from the material changes were measured in the time domain. The sound amplitude is expressed as the ratio of the sound pressure to standard reference of acoustic pressure where water, air and oil are the differentiators [42]. As it is introduced into the pipe, the fluid expands and creates sound vibration which in turn produces high peak at its natural signal. Sound signals were recorded in the time domain and as expected, the highest flow rate produces the highest voltage amplitude. The data was analysed in time domain, as can be seen in Figure 5. The dominant sound sample was always present even when different rates are being introduced confirming that both fluid density and flow increment resulted in changing peaks albeit within the same time signal bands.

Figures 5 A and Figure 5 B were distinctive for water. The background noise comparison exists as the small peaks and therefore found that the range for water was between 500 mV to 800 mV for every 10 seconds of the sound signal recorded. Different fluid has a unique time signal at which it resonates, which goes the same for air and oil. The S/N ratio indicates that the signal's amplitude rising and shift density correlated to the increased flow rate. The experiment was repeated using oil. Thus, a similar correlation was identified in that the sound amplitude increased with the flow rate. With the known confidence, different densities will result in different speeds [26]. The peak sound level was the highest for water and can be explained due to the higher density of the water. The oil sound level was found to be relatively small with peaks that appeared to be non-existent at this resolution in comparison with water.

The wavelength variation was dependent on the change of flow rate and pressure. Low pressure gave rise to a linear difference in the wavelength change. As a result, the strain of the pipe could be determined knowing that the fluid velocity is proportional to the internal pressure growth. From Figure 5 A to Figure 5 B, the difference between acceleration conditions can be distinguished by a slight change. This indicated that it was not enough to excite and cause external energy release, which is sensitive to the output voltage and certain force acting on the pipe. The transitional change associated with increased flow or stress in the pipe corresponded to an increased strain and force from induced pressure. As the transitional region was transferred between flow rates, there was a slight Bragg wavelength shift as a result of a circumferential disposition of internal pipe pressure and stress distribution. Even at low flow rates (13 l/min), the change in Bragg wavelength was seen to be corresponding to the change in pressure. This is significant as it demonstrated that the system could operate at low flow rates, giving good resolution.

Water was at an equivalent flow rate as the oil and had higher sound amplitude as flow rate increased. This showed that sound peaks were related to the flow rate of both fluids but different due to density changes. The top and bottom sensors displayed a correlation of induced strain from the FBG sensors and strain gauge values, demonstrating a linear AE relationship with the strain result. This further validates the sensor results using a multi-spectral approach. With higher flow rate, the magnitudes of the AE peak to peak were higher, in correlation with greater pressures. The transition in flow rate from 13 l/min to 18 l/min (Figure 5 C to Figure 5 D) demonstrated that there was a significant AE response to an increase in pressure, as the flow rate increased. For high pressure and higher flow rates, the AE response showed more dense bursts of signal. The values of which were then correlated to a flow meter and the AE response showed a corresponding change in flow rate. This also correlated with an increase in wavelength shift change from the optical FBG which was proportional to an increase in flow rate.

In Figure 5 A and Figure 5 C water sound waves in water had similar peak distributions as oil of around 300 mV – 400 mV and oil, in comparison with water, produced a different sound range. The shift density of the signal dropped to 200 mV between water and oil as this indication showed a lower spheroidic energy release obtained for a denser liquid. This is because the density of oil is lower compared to water therefore the phenomenon that was recorded was higher in sensitivity, as it also depends on the pressure and their volume introduced. This inclusion is the result of higher amplitude rise with more dense liquid and due to the speed of propagation and the amount of energy received. The dynamic wavelength shifts resulted in lower peak amplitudes, from the comparison of 60% water to 41% oil at the same flow rate, due to differences in density [26].

The difference in amplitude in Figure 5 B and D, both at constant 26 l/min showed that a higher liquid velocity produced a higher sound peaks in the form of a more significant peak. The same is true for the sound signal recorded between water and oil as the energy release would have been greater with the introduction of higher flow rates. From the calibration process, the accelerometer posed certain limitations towards vibration lower limits to measure the actual vibration of the pipe, thus conforming the actual change in strain through circumferential disposition from an increased flow. The sudden changes of the Bragg wavelength, which is the mean in transition evaluated through strain acting on the fibre. Throughout this work, it has been shown that the non-intrusive flow sensing system can sense low flow rates (between 13 l/min to 26 l/min). As a result of higher flow speeds (> 26 l/min), more significant wavelength shifts would be expected from the force-induced strain meaning that this system could be used for higher flow rates for Reynolds Number higher than 4000.

Fuzzy clustering from an unsupervised technique for blind segregation of leakage data

The abnormal flow pattern shown in Figure 6 from the dotted oval lines was the result of an acoustic signal associated to the change of normal pattern flow of the water. This can be associated with a sudden increase in strain which can be caused by a change in fluid flow. As can be taken from Figure 6, the average acceleration correlated with increased pressure from an increased strain.

At point A, in Figure 6, the peak can be linked to the start of when the leakage occurred as the rest of the peaks are nominal from the event introduced in real time. Due to the pressure existing inside, the liquid was forced out to create an equilibrium with outside and this can be categorised as cavitation which in turn tells us that the spikes are the representation as the rate of leak. When compared to the pencil calibration, and repeated tests data in Figure 2, indication of when fluid passing was noted, causing spikes rising to 1.4V, as seen from Figure 6. Similarly, in the work done by Husin and Alhashan [33, 38], the Authors have explained cavitation and bubble collapse which is smaller than then pencil calibration test. In [38], The AE-RMS and threshold levels are said to be sensitive for monitoring bubble activity and movement towards water surface. From their observation, the bubble formation was detectable when standard analysis techniques including RMS hits and threshold levels where applied. In another work done by Essid [39], the AE emitted was said to be proportional to the quantity of the solid particle as the impact showed to not often generate large or medium AE signals between solid particles, with an increase flow rate. This increased the velocity of solid particle in stream which increased the kinetic energy resulting in an increase of the AE signals. The conclusion signifies that the sound waves generated could have resulted from those spikes and correlating leakage phenomenon [34-36].

The Fourier transform for both sensors to the original signal from Figure 7 showed that sensor 2 resulted in a factor of 2 difference in terms of amplitude when compared to sensor 1 from the same frequency band; therefore, sensor 2 is picking more energy in total duration, and the shift was slightly higher in terms of phenomena when compared between both sensors. Energy is released more in the bottom sensor; from the utilisation of the graph, both sensors pose similarity, but the amplitude for sensor 2 is 10 times more significant from the top sensor (sensor 1), and the frequency band has shifted by a slight change where the prominent peak is 0.4 MHz as compared to 0.3 MHz deducing the noise factor and ignoring anything above 1 MHz There seemed to have more frequency shift on the bottom sensor in terms of amplitude and frequency comparison. As it gets further to the top, it started to collapse from the dispersed molecules resulted in the energy being released.

The continuous file stream in Figures 11 showed a rich summary description model for the set of targets to the multidimensional data points of the raw leak data allowing apparent discrepancy between sensor 1 (closest to leak phenomena) and sensor 2 implemented as ΔdB, the clustering method applied distinguished the features/difference. The technique that was applied here is the reduced down, descriptive data (rich summary of data nuggets). The algorithm comprises principal component analysis to show most data significance towards the *x* and *y* data. This section will investigate different data variations (S1-S2=Δ1), differentiating the top and bottom sensor. Principle component analysis is within the algorithm, which means the most significant deltas are used over the others. By using the deltas, there was a difference between the leakage and non-leakage; without the use of deltas, there appears to be no change in noise. The blind classification showed which data is more significant in breaking up a leak and non-leak. The calibration process was taken as a point of reference and was normalised for consistency towards a leak and no leak data; the average peak recorded for each scenario was at a constant 80 dB and averaging 200-300 counts as seen in Figure 8. The calibration pencil lead breaking fracture was carried out five times, and the average was taken, following this procedure. The repeated tests showed similar positioning and damping. There was confidence in the fixed sensor positioning and towards the final reading.

From the continuous file stream, there was verification that the mechanical data, the flow was low, and it was picked up at such low amplitude. Compared to the leak, the no leak (Figure 9) had a more significant peak of around 55 dB at the range of 20-40 hits. On the opposite side, leak data (Figure 10) were lower, recorded at 45 dB but higher hits 60 -80. AE data were able to detect a small flow change from the bottom sensor where leakage occurred, even though it was slightly lower when compared to the leak data (this could also mean that the energy is dispersing/dissipating through the leak). The notable data could also mean that the result picks up apparent leak, which is smaller, recording water droplets.

Raw data defined as the duration of time was much higher for no-leak compared to leak. In other words, there were more spikes in the leak as the duration is much smaller; from this observation, a good discriminator between the variables can be chosen. As seen from Figure 11, there were not many events happenings to look at the amplitudes (y-axis); however, the amplitude was relatively high in the case of no leak. The possible explanation would be that the sensors (with good contact and calibrated) from Figure 8 and Figure 10 when there is no leak, the pressure remained the same, so any movements from the pressure and the pump remained the same noise. Therefore, the elastic waves that were initiated from pipe material were the same, which doesn't change from sensor 1 (top position) and sensor 2 (bottom position). From the minute leak that was recorded, the pressure was released. With a slight noise in comparison to a no-leak scenario, there were notable differences. The segmentation of cluster centres presented in Figures 11 is defined by the value of data points assigned by the algorithm. From the original data, it can be said that no leak defines the lower data points in the clustering results. Going higher data point values is the tending towards a leak and definite leak. Their respective colour centroids call out these identifications. The negative value in x and y is defined as how the algorithm segregates the data based on its Euclidean distance. Nevertheless, it is assumed to have a positive value throughout (from the data perspective).

In Figure 11, red centroid (fuzzy centre) is defined as locally supported, the relevance/similarities compact together. The marginal points (blue) from where the similarities were seen less and lastly, the difference with the green centroid, green marker, therefore, can be grouped as no leak, blue as the start of the leak, and red is a definite leak which was based on the sensors picking up relevant data. The data was tending towards leak for the grouping of all different points towards leak data. Cases in the middle based on the numbers would suggest that this was the start of the leak as it is tending more towards a more compacted clustering feature on the left-hand side of the graph. The energy was reduced compared to the energy (which was relatively high) on the right-hand side cluster (grouped as no leak).

The algorithm barrier defined the clusters as leak and no leak showing discrepancy in the middle graph, P9, P10, P16, P29, to name a few tending towards 'start to leak' picked up from the sensor. For leaks, two peaks were observed. The first peak can be said that the sensor picked up pressure within the system, the other peak seen possibly from the leak itself where the water was released. There were noises present from the pump and other operating mechanical disturbances which were more prominent, but smaller peaks were recorded, different, notable from phenomena of the leak and no leak. From the results shown, the cluster for a definite leak can be seen to have good, localised data support. Based on the Euclidean distance from the 2 dimensions, between -2dB and 2dB changes were locally supported, and the leak state was observed. The energy here was dissipating (reading less of energy signal, as it was dissipating). The clusters formed to strengthen the fusion approach of identifying the unsupervised leak outlier data based upon primary reading extracted from the multi-spectral approach and using AE to characterise structural health upon the change in flow readings [43-45].

Taylor Bubble: Flow characteristics through Acoustic Emission (AE)

In multi-phase flows, it can be difficult to distinguish flow patterns and types. A sample AE measurement under flow conditions is presented in Figure 12 and Figure 13. The AE sensor was non-invasively placed and mounted on the surface of the pipe wall via an adhesive coating and a contact film promoting signal propagation. The sensitivity of the sensor was then evaluated using Hsue- Nelson pencil lead break fracture technique [31]. The levels of AE energy recorded from the sensor under the flow condition showed the level of AE signal increased from point A to point B, as the bubble passing elongation tended from low to high from what is seen in point C. Largest amplitude that was associated with the largest developed bubble and lowest energy burst released was entirely based on the fluid region (see Figure 13). The AE levels that were associated with the density and viscosity discussed previously were as expected, having to consider the rate of bubble collapse. Also, it was seen that the bubble was bigger than the body of pattern regime as it passed from the bottom sensor to top sensor, which in turn signified the gas phase, assuming the bubbles are all discrete [24]. This enables the identification of the bubble regime as the bubbles pass the AE sensor.

As the flow rate increased it created a consecutive bubble causing shape oscillation. The signals were picked up by the sensor when noise activity passed a certain threshold (in this case 40 dB). As the bubble collapsed, bubble oscillation during its journey to the surface was observed. The bubble formation and burst detection showed an increasing bubble size from one region in the pipe to another. With an increase in bubble size, AE amplitude bursts also increased. This indication can be applied where different liquid viscosity affects AE signals. The sound emitted was dependent on the size of bubble, stress pulse, density and associated liquid damping factor affecting the signal propagation and attenuation and also, the pinch-off (drop release) from the time it was recorded.

At a fixed rate, increasing gas velocity was the result in an increase of measured absolute AE energy. At a fixed distance between the top and bottom sensors, the velocity of the acoustic wave in liquid increased with the increasing size of bubble burst. The average velocity of the AE wave was higher in water compared to oil, showing that liquid viscosity and density was notable in multi-phase liquid. The results, as seen in Figure 13, showed a larger bubble size gave rise to a greater AE amplitude and count which is proportionate with both bubble size and liquid viscosity.

This would enable the non-intrusive flow sensing system to detect differences in liquid characteristics and bubble characteristics.

Conclusions

Through the experimental investigation of two-phase flows in vertical pipes, a multi-spectral approach enables efficient identification and characterisation of fluid density, pressure, and bubble formation. The implementation of strain gauges, optical fibre Bragg gratings (FBGs), thermocouples (K-type), accelerometers, acoustic emission analysis and gyroscopes, as a multi-spectral approach can be used to study two-phase flow. The sensor configurations that were adopted demonstrated the technique and cross effect study of health monitoring and understanding the structural integrity of a pipe accounting for numerous pipe health and flow parameters. The system proposed is non-intrusive, it can be installed to existing pipes and does not affect normal operation. The sensors further interconnected through data processing forming a fusion sensor network that can relay information from collected data in real time. The sensors are correlated to their measurements, assessing whether the drop in fluid velocity was caused by the leakages.

The amplitude of the strain signals acquired resulted to a linearly proportional relationship to the measured flow rates, by the correlation of the sensors positioned on the pipe wall to measure flow rate, is presented for different valid speeds of signal; showing the amplitude of flow increases as the flow rate increases. The sensor adopted allows measuring flow without the physical contact and interaction with the liquid being measured. The technique applied through the multi-spectral approach can distinguish between single and two-phase liquid/air through the change in density. Furthermore, a leak was detected through non-intrusive monitoring, with an accurate signal 'footprint' to segregate leak behaviour. The velocity of oil increased as oil viscosity increased and decreased when the oil viscosity reduced. Oil had slightly better transmission than water. For most data, this can be distinguished with little ambiguity. The maximum flow rate introduced showed the change of pattern correlation. Flow velocity and physical properties of different fluids influence sensor accuracy. The multi-spectral data recognise the multi-phase flow conditions and how that is associated with the actual strain, acceleration, and overall physical property of the pipe, leading to recorded anomaly data. The pressure difference was seen when the oil viscosity and velocity increased, as flow velocity and change in density both influenced the signals recorded.

The relationship between the sound peaks and fluid flow rate was examined for both air and liquid through experimental observations. Sound generated by fluids moving through a pipe and into a vertical well were found to have dominant time signal range for different fluid phase. The sound's magnitude indicated sound amplitude, and flow rate increased with flow rate for liquid/air, and the overall dominant peak time signal for each sound recorded indicated the fluid phase. The clustering algorithm was able to segregate leak and no leak data, correlating AE through early detection of the anomaly when the leak first occurred and the occurrences following that event. The anomaly and changes due to fluid flow, impact towards leak phenomenon was exerted towards the structural health of the pipe. In the future work, the implementation of using AE detection to study two-phase flows will be to look at different sizes of aperture and to adopt the technology towards an automated system.

Declaration of interests

On behalf of all authors, the corresponding author states that there is no conflict of interest.

References

1. B. F. Spencer and M. Ruiz-Sandoval, "Smart Sensing Technology for Structural Health Monitoring," in Earthquake Engineering , Canada, 2004

2. Alsaka Department of Enviorment Conservation (2004) 'Technical Review of Leak Detection Technologies Crude Oil Transmission Pipelines'

3. P. Cawley, "Structural health monitoring: Closing the gap between research andindustrial deployment," Structural Health Monitoring , 2018

4. Abd Murad, M. (ed.) (2009) *4th European-American Workshop on Reliability of NDE*. 'The Development of Structural Health Monitoring (SHM) Procedures for the Structural Integrity and Maintenance Repair of Offshore Ageing Pipelines ': NDT net

5. J. Li, X. Yang and R. Sitzenfrei, "Rethinking the Framework of Smart Water System: A Review," Water, vol. 412, no. 12, p. 25, 2019

6. F. Dai and D. Wang, "Analysis and Comparison of Long-Distance Pipeline Failures," Journal of Petroleum Engineering, 2017

7. A. Santos and M. Younis, "A sensor network for non-intrusive and efficient leak detection in long pipelines," in Proceedings of the IFIP Wireless Days Conference, Canada, 2011

8. P. Hopkins, "PIPELINES: Past, Present, and Future.," in Asian Pacific IIW International Congress, Sydney, 2007

9. S. Zahab and T. Zayed, "Leak detection in water distribution networks: an introductory overview," Smart Water, 2019

10. Trans Mountain Pipeline spill in Abbotsford estimated at up to 190,000 litres of crude oil. CBC.ca. Retrieved 02 May 2021

11. 9. A. MacLean and C. Moran, "Detection of hydrocarbon fuel spills using a distributed fibre optic sensor," Sensors and Actuators A Physical, p. 7, 2003.

12. Colombo, A. and Karney, B. W. (2003) 'Pipe Breaks and the Role of Leaks from an Economic Perspective'. *Water Science & Technology. Water Supply* 3 (1-2), 163-169

13. Zou, L. & Sezerman, O., 2008. Pipeline Corrosion Monitoring by Fiber Optic Distributed Strain and Temperature Sensors. NACE International, pp. 1-8.

14. Barry, A., Broaddus, D. & Ivasauskas, J., 2015. A Novel Solution for Performing Real- Time Fiber Optic Temperature Measurements. SPE International, Volume 175047- MS, pp. 1-18.

15. Bolognini, G., Soto, M. A., and Di Pasquale, F. (2010) 'Simultaneous Distributed Strain and Temperature Sensing Based on Combined Raman–Brillouin Scattering using Fabry–Perot Lasers'. *Measurement Science & Technology* 21 (9), 094025

16. Bado, M. F. and Casas, J. R. (2021) 'A Review of Recent Distributed Optical Fiber Sensors Applications for Civil Engineering Structural Health Monitoring'. *Sensors (Basel, Switzerland)* 21 (5), 1818

17. A. Cataldo and G. Cannazza, "A New Method for Detecting Leaks in Underground Water Pipelines," IEEE Sensors, pp. 1660-1667, 2012

18. Adegboye, M. A., Fung, W., and Karnik, A. (2019a) 'Recent Advances in Pipeline Monitoring and Oil Leakage Detection Technologies: Principles and Approaches'. *Sensors (Basel, Switzerland)* 19 (11), 2548

19. Ahadi, M. and Bakhtiar, M. S. (2010) 'Leak Detection in Water-Filled Plastic Pipes through the Application of Tuned Wavelet Transforms to Acoustic Emission Signals'. *Applied Acoustics* 71 (7), 634-639

20. Inaudi, D. & Glisic, B., 2010. Long-Range Pipeline Monitoring by Distributed Fibre Optic Sensing. Journal of Pressure Vessel Technology, 132(011701-1).

21. Barry, A., Broaddus, D. & Ivasauskas, J., 2015. A Novel Solution for Performing Real- Time Fiber Optic Temperature Measurements. SPE International, Volume 175047- MS, pp. 1-18.

22. Brown, g., 2009. Downhole Temperatures from Optical Fiber. Oilfield Review, 4(20), pp. 34-39.

23. Cusano, A., Breglio, G. & Giordano, M., 2001. Fiber Optic Sensing System for Smart Materials and Structures. IEEE, pp. 1401-409.

24. Besagni, G. & Inzoli, F. 2018 Two-Phase Bubble Columns: A Comprehensive Review. MDPI, Chemengineering

25. Fang, L., Yang, Y., Fu, L., Wei, Z., Zhao, N., and Li, X. (eds.) (May 2018) . 'The Noise Characteristics of Gas-Liquid Two Phase Slug Flow in Vertical Pipe': IEEE

26. 18. Pan, Y., Chen, Z. & Xiao, L., 2010. Application of Fiber Bragg GRating Sensor Networks in Oil Wells. SPE International, Issue 136978, pp. 1-6.

27. 19. Wang, W., Song, H. & Xue, J., 2011. Overview of Intelligent Composites with Embedded FBG Sensors. IEEE, pp. 47-51.

28. Lawrence A. Klein (2012) 'Multiple-Sensor System Applications, Benefits, and Design Considerations'. in Sensor and Data Fusion: A Tool for Information Assessment and Decision Making, Second Edition. ed. by Anon: SPIE Press, 9-52

29. Ho, J. S. and Li, Z. (2015) Microwave Metamaterials for Biomedical Sensing.: Elsevier Inc

30. Liptak, B. (2021) Do Multiple Sensors Improve Accuracy? [online] available from <https://www.controlglobal.com/articles/2018/do-multiple-sensors-improve-accuracy/> [04/11/ 2021]

31. N.N. Hsu, F.R. Breckenridge 1981, Mat. Eval., 39, 60-68

32. El-Alej, M. E. (2014) Monitoring Sand Particle Concentration in Multiphase Flow using Acoustic Emission Technology. [online] thesis or dissertation

33. Husin, S& Addali, A. 2010 Acoustic Emission for monitoring two-phase flow. EWGAE Vienna

34. Bernasconi, G. and Giudice, S. (eds.) (2012) . 'Pipeline Acoustic Monitoring '

35. Droubi, M. G., Reuben, R. L., and Steel, J. I. (2018) 'Flow Noise Identification using Acoustic Emission (AE) Energy Decomposition for Sand Monitoring in Flow Pipeline'. *Applied Acoustics* 131, 5-15

36. Droubi, M. G., Reuben, R. L., and White, G. (2012) 'Statistical Distribution Models for Monitoring Acoustic Emission (AE) Energy of Abrasive Particle Impacts on Carbon Steel'. *Mechanical Systems and Signal Processing* 30, 356-372

37. Shuib, H. & Mba, D. 2010 Acoustic Emission of a Single Bubble Activities Proceedings of the World Congress on Engineering 2078-0958

38. Alhashan, T. & Addali, A. 2018 Experimental investigation of the influences of different liquid types on acoustic emission energy levels during the bubble formation process, Int J Energy Environ Eng 9:13–20

39. Essid, M. 2014 Monitoring Sand Particle Concentration in Multiphase Flow Using Acoustic Emission Technology, PhD, Cranfield University, Cranfield

40. Narcy, M. and Colin, C. (2015) 'Two-Phase Pipe Flow in Microgravity with and without Phase Change: Recent Progress and Future Prospects'. *Interfacial Phenomena and Heat Transfer* 3 (1), 1-17

41. Alssayh, M. & Addali, A. 2013 Identification of Two-Phase Flow Regime Using Acoustic Emission Technology. International Journal of Mechanical and Production Engineering

42. 41. Griffin, J. 2014, Traceability of Acoustic Emission measurements for a proposed calibration Method – Classification of Characteristics and Identification using signal analysis, Mech. Syst. Signal Process. Volumes 50–51, Pages 757–783.

43. Gath, I. and Geva, A. B. (1989) 'Unsupervised Optimal Fuzzy Clustering'. *IEEE Transactions on Pattern Analysis and Machine Intelligence* 11 (7), 773-780

44. Gosain, A. and Dahiya, S. (2016) 'Performance Analysis of various Fuzzy Clustering Algorithms: A Review'. *Procedia Computer Science* 79, 100-111

45. Klawonn, F. (2008) 'Fuzzy Clustering: Insights and a New Approach' 11 (2-3)

Table 1: Dynamical characteristics of different vertical upward water-oil flow patterns and sensor response; at fixed volumetric flow rate 13 l/min. Comparing similar fluid systems (oil-water interfacial tension).

Water (Top sensors)	Oil (Top sensors)	Water (Bottom sensors)	Oil (Bottom sensors)
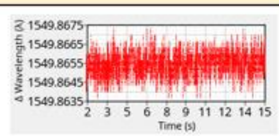	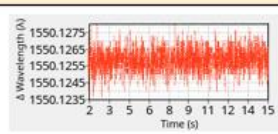	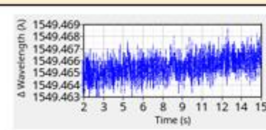	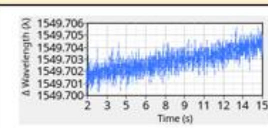
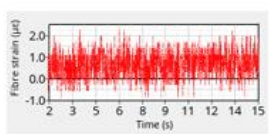	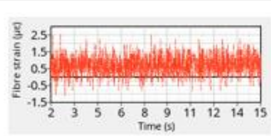	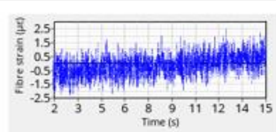	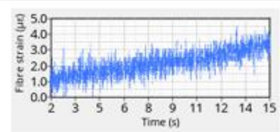
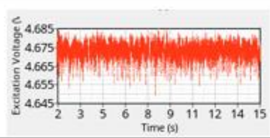	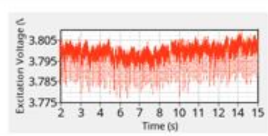	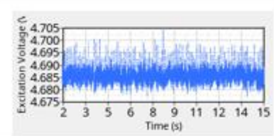	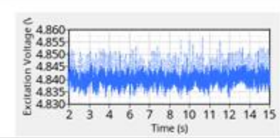
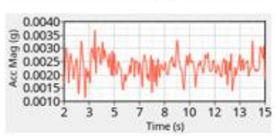	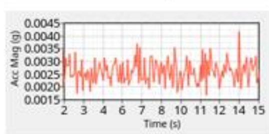	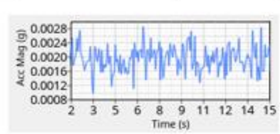	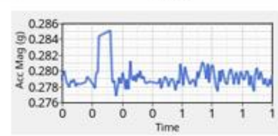
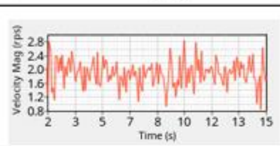	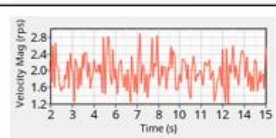	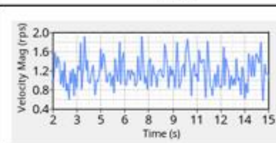	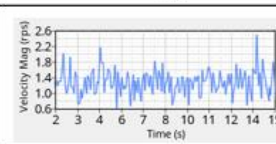

Table 2: Dynamical characteristics of different vertical upward water-air flow patterns and sensor response; at fixed volumetric flow rate 13 l/min. Comparing similar fluid systems (water-air interfacial tension).

Water (Top sensors)	Air (Top sensors)	Water (Bottom sensors)	Air (Bottom sensors)
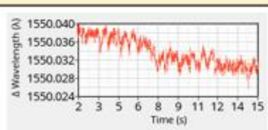	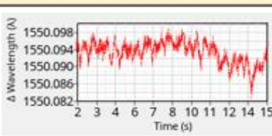	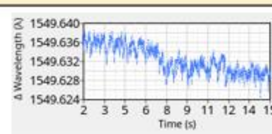	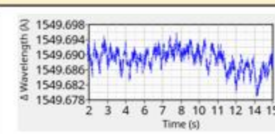
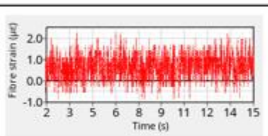	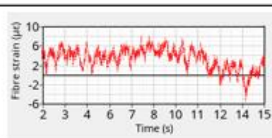	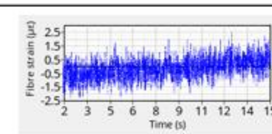	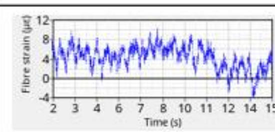
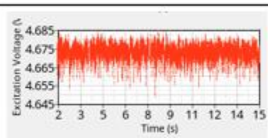	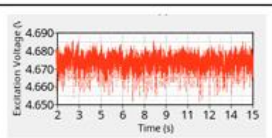	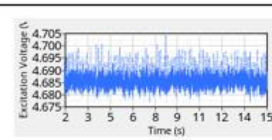	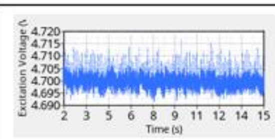
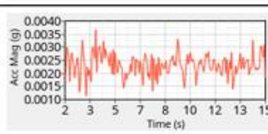	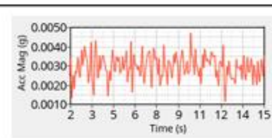	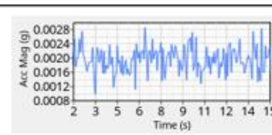	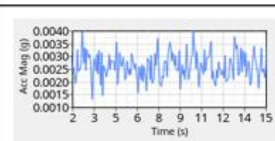
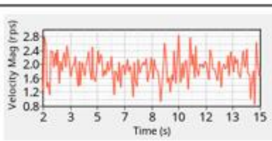	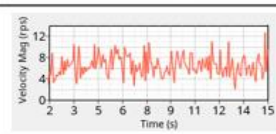	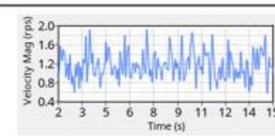	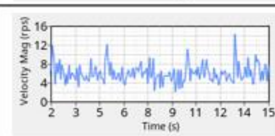

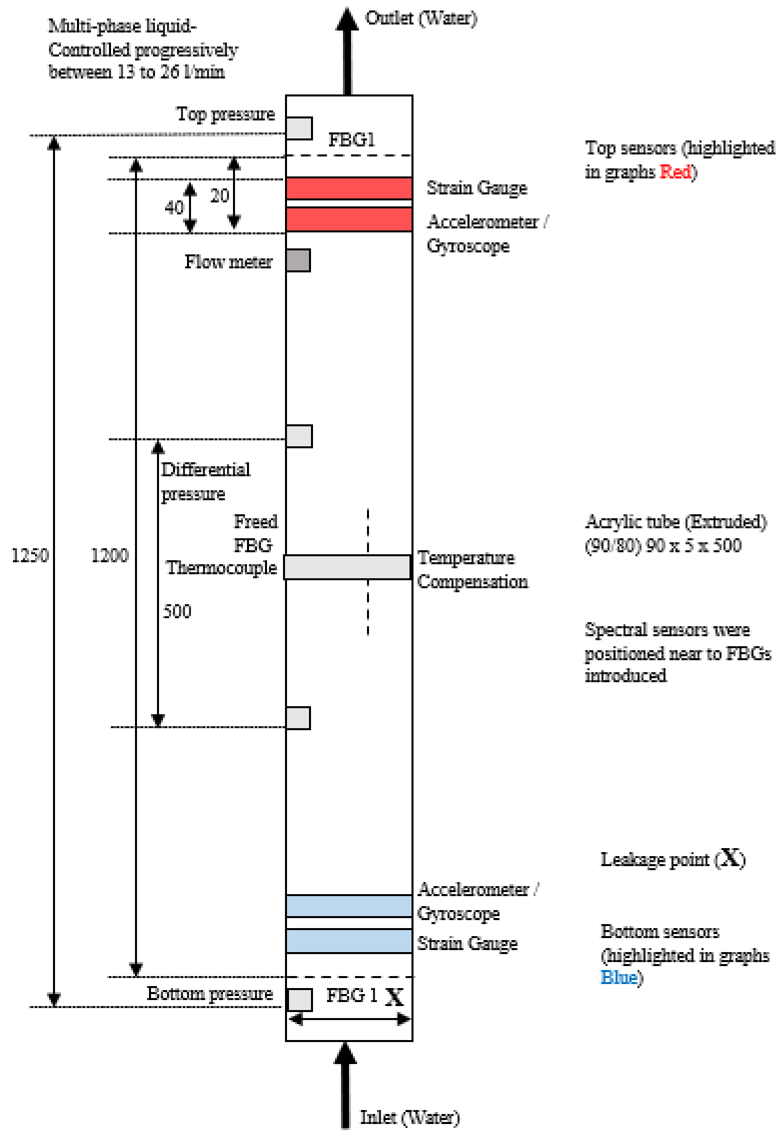

Figure 1: The multiphase flow rig. The sensors were in proximity of specific distance configured at 1200 mm between top and bottom sensors.

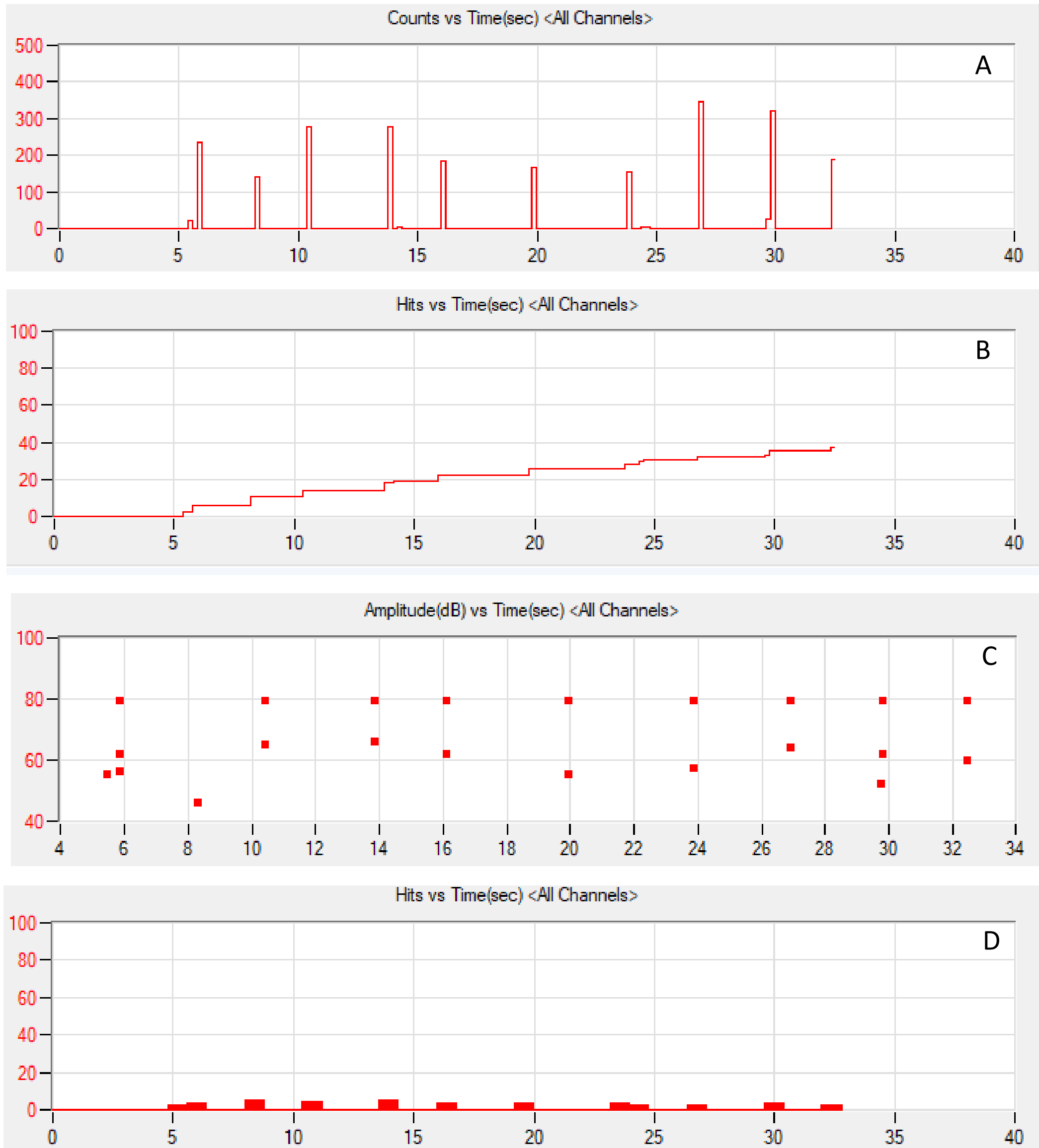

2: Hsu-Nielson pencil break calibration results.

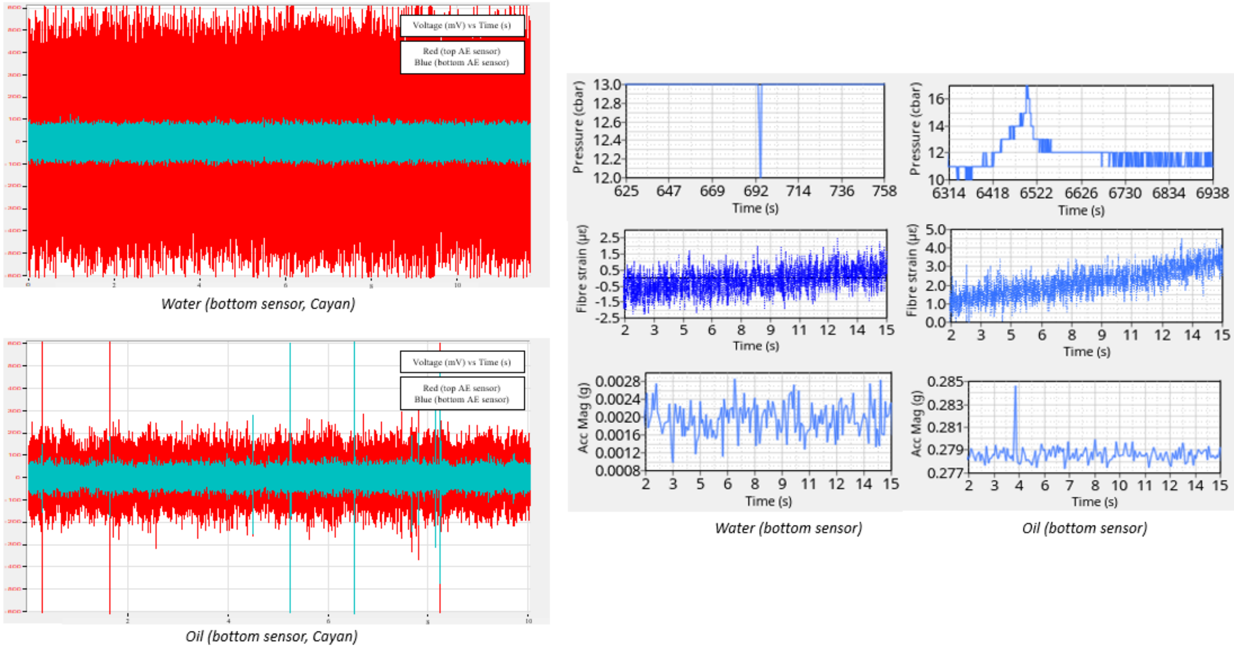

Figure 3 Cross-correlation signal profiling; comparing measured phase volumetric flow rate. Measurement was able to detect at a different density from the transitional boundary between oil and water.

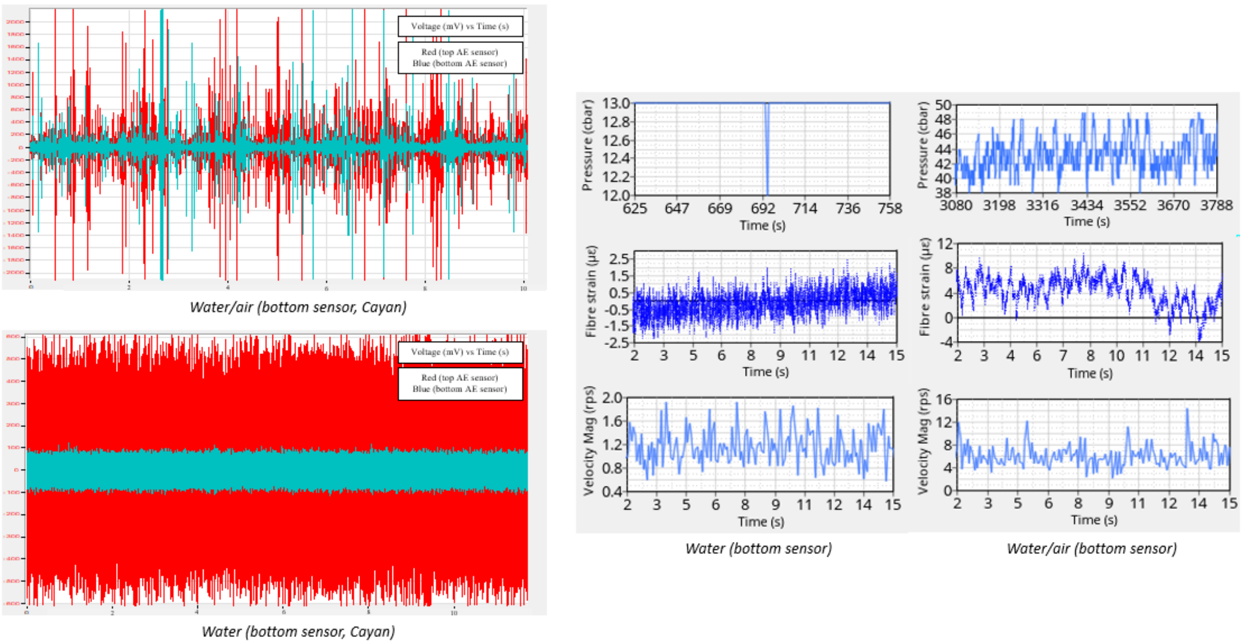

Figure 4: Cross-correlation signal profiling; comparing measured phase volumetric flow rate. Distinguish between single and two-phase liquid/air, with an introduction of bubble formation detected by AE.

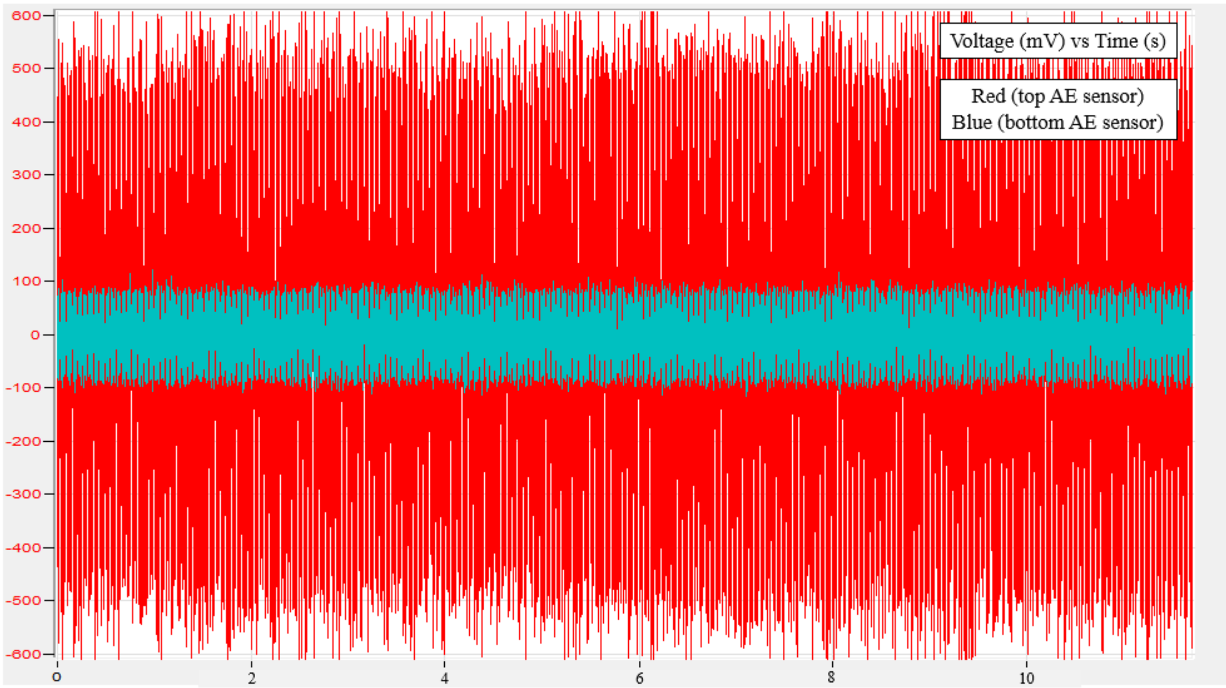

5 (A): Sampled sound signal in the time domain: 13 l/min (water)

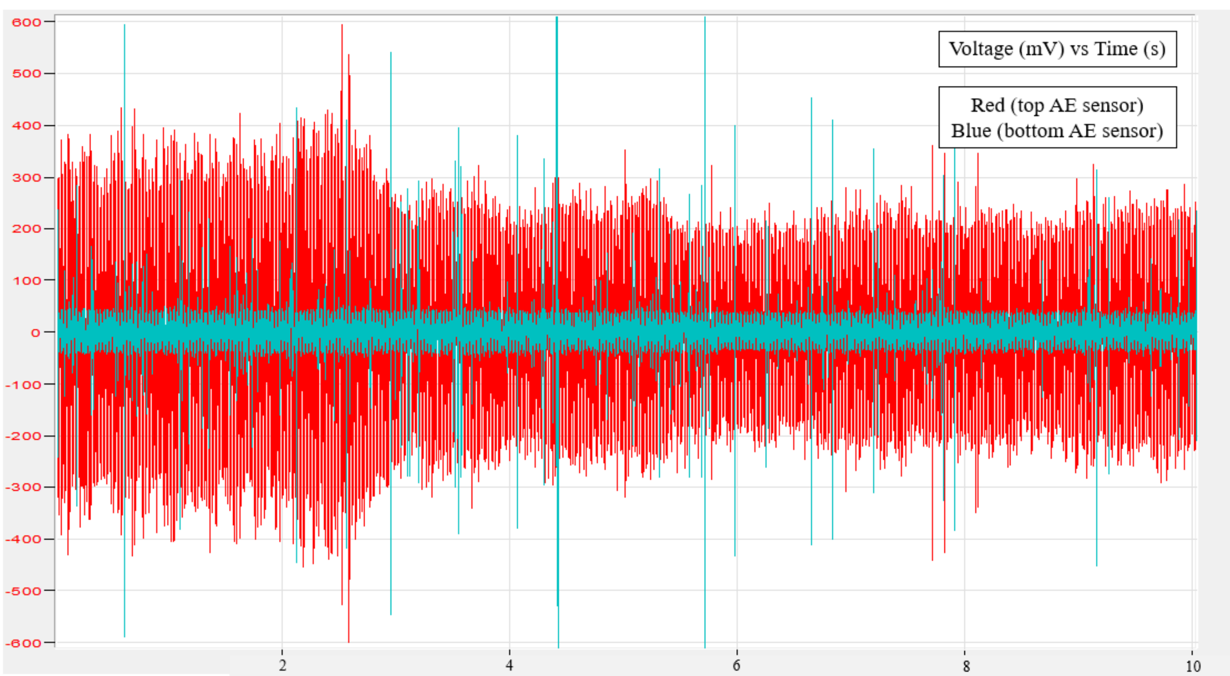

5 (B): Sampled sound signal in the time domain: 26 l/min (water)

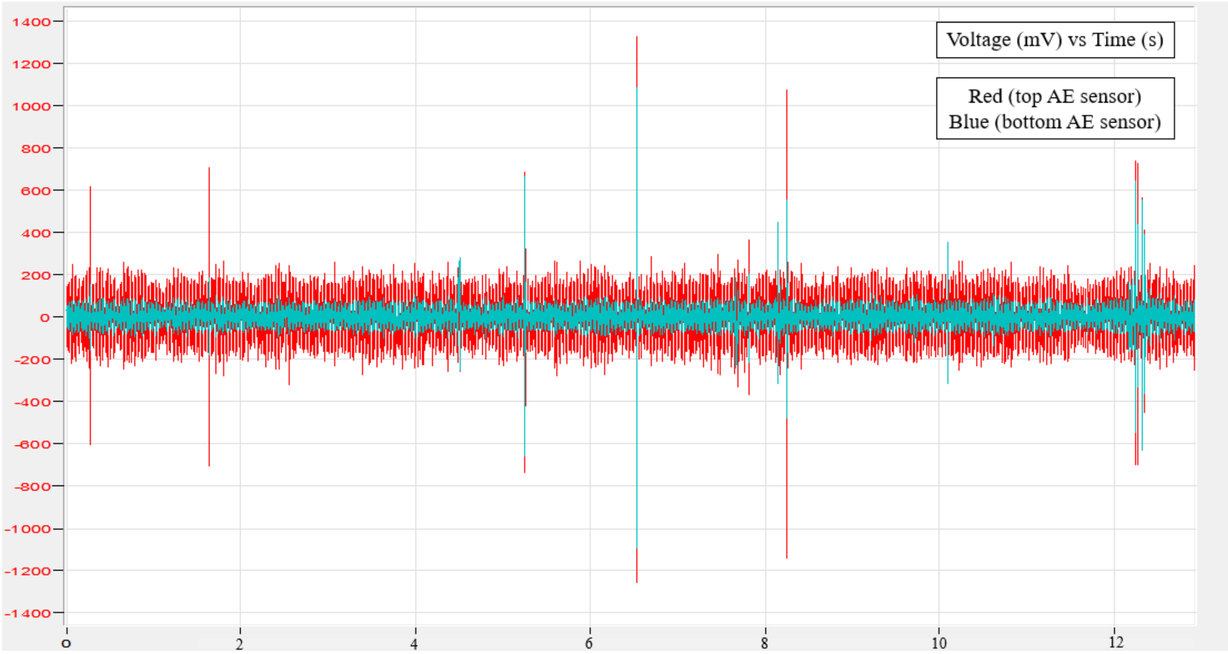

5 (C): Sampled sound signal in the time domain: 13 l/min (oil)

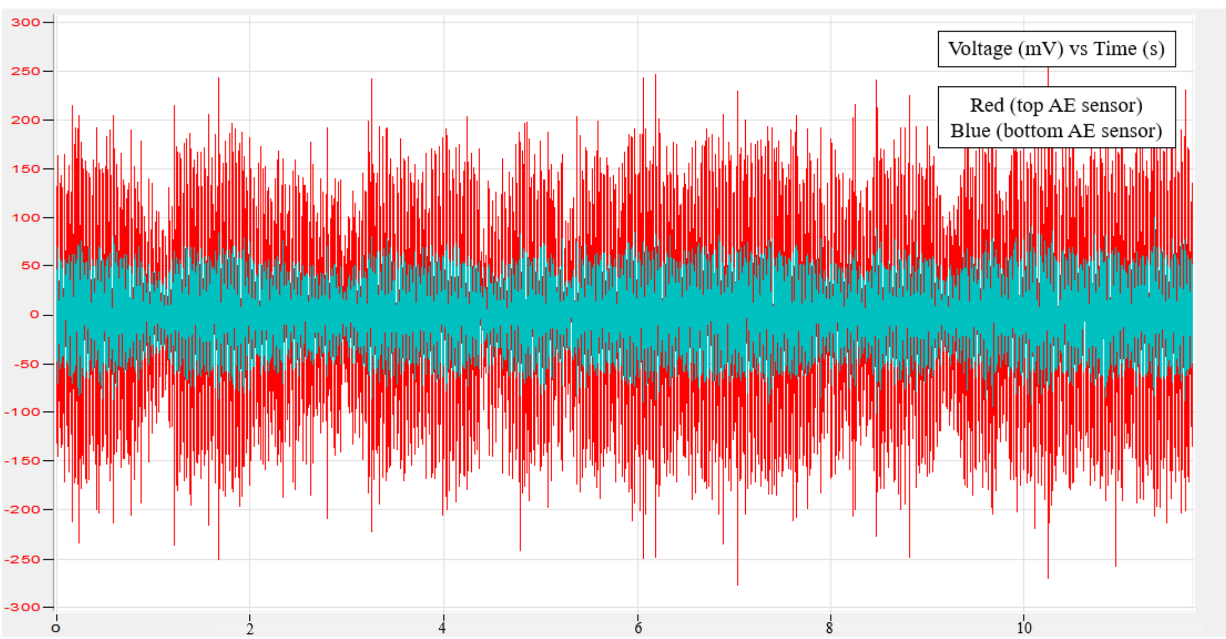

5 (D): Sampled sound signal in the time domain: 26 l/min (oil)

Figure 5: Voltage (mV) against Time (us): The magnitude of sound produced indicates the fluid flow rate and dynamic pattern properties from the acoustic data.

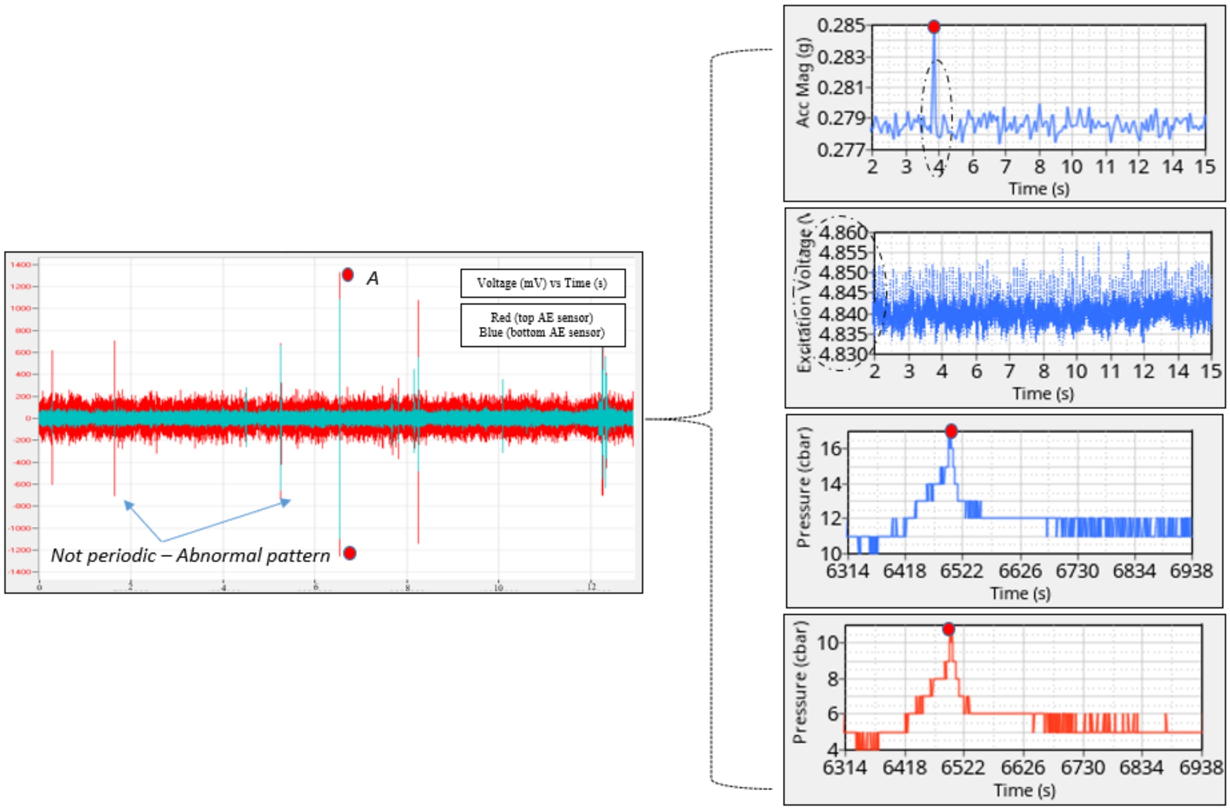

Figure 6: Comparison of peak distribution for water. The dominant peak of sound spectrum indicates the fluid phase and leakage scenario; Sampled sound signal in the time domain: Comparison of peak distribution for the start of leak. The sound spectrum dominant peak indicates the fluid phase and leakage scenario.

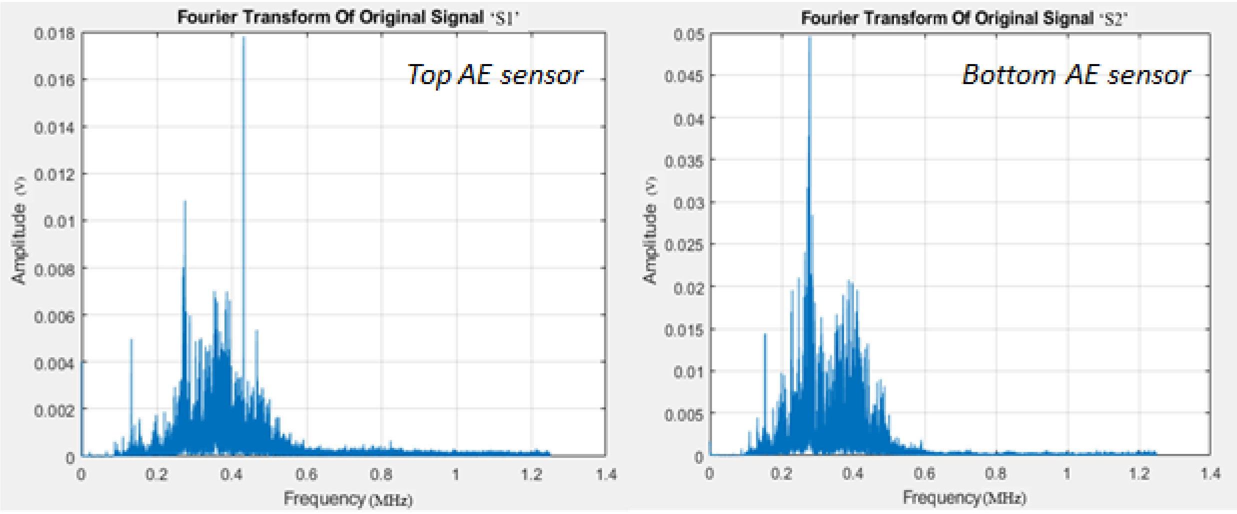

Figure 7: Frequency response for top and bottom sensors towards leak data, indicating more energy release in sensor 2.

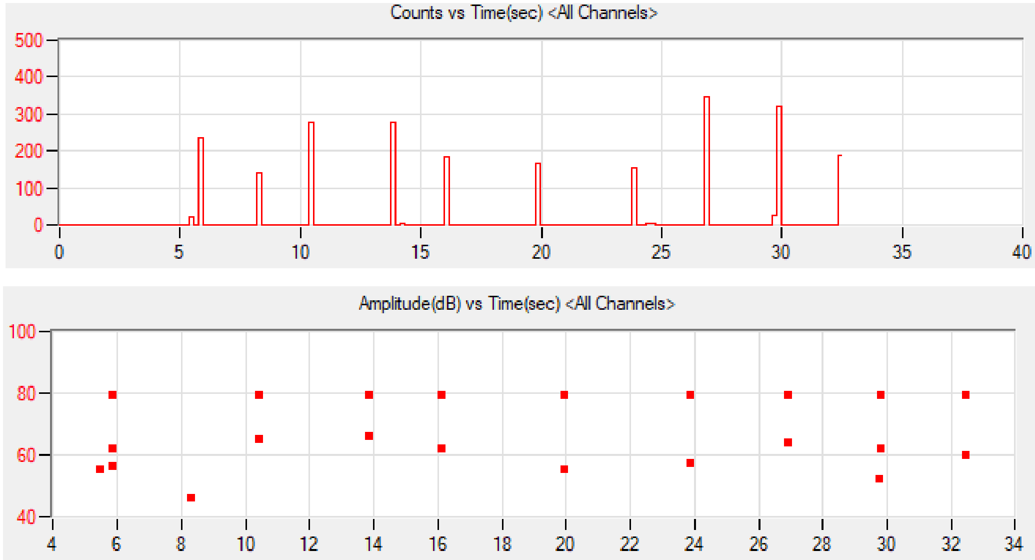

Figure 8: Hsu-Nielson pencil break calibration results taken when leak occurred. [RW.ERROR - Unable to find reference:doc:60fe7ce58f08f5deb409b98b].

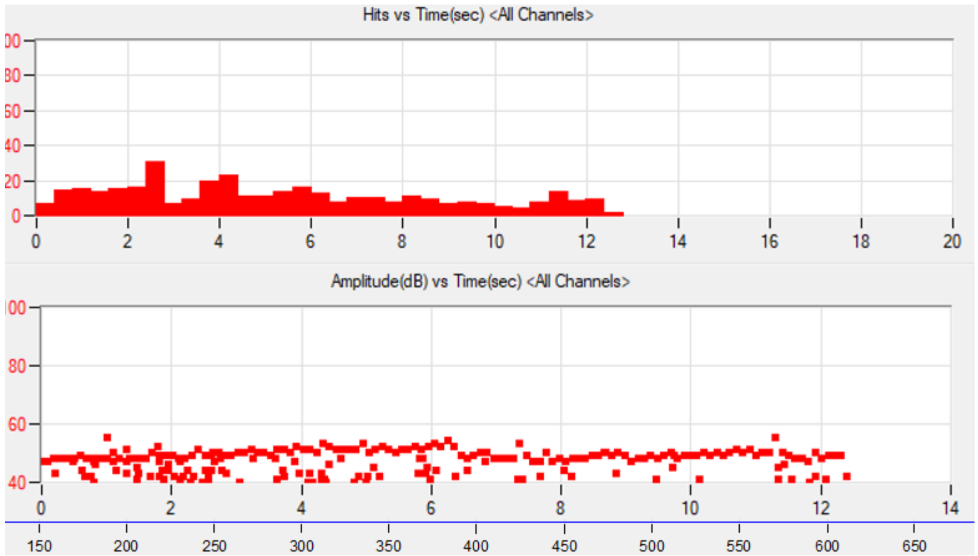

Figure 9: Signal parameter of a non-continuous/multi-parameter file stream for Hits and Amplitude (dB) against time, for non-leakage data.

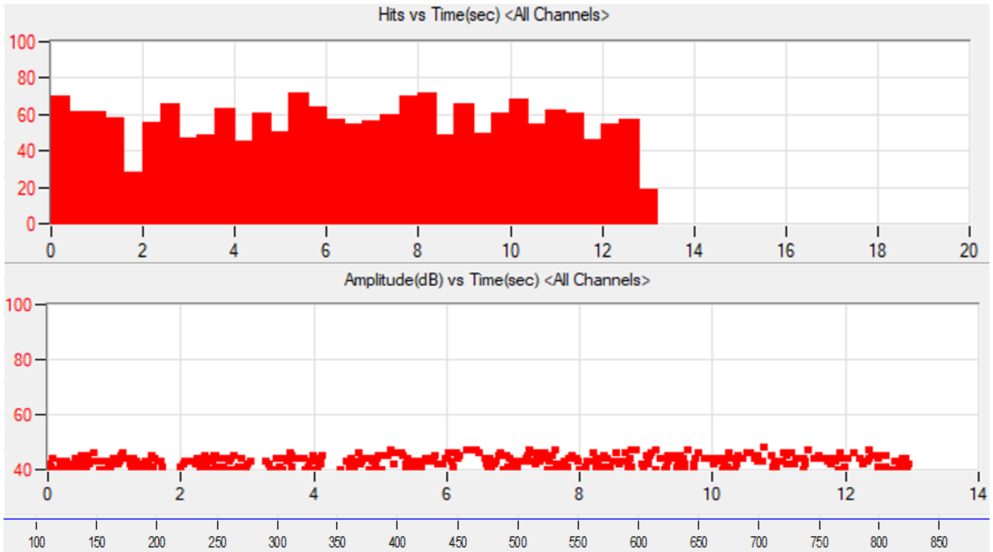

Figure 10: Signal parameter of a non-continuous/multi-parameter file stream for Hits and Amplitude (dB) against time, for leakage data.

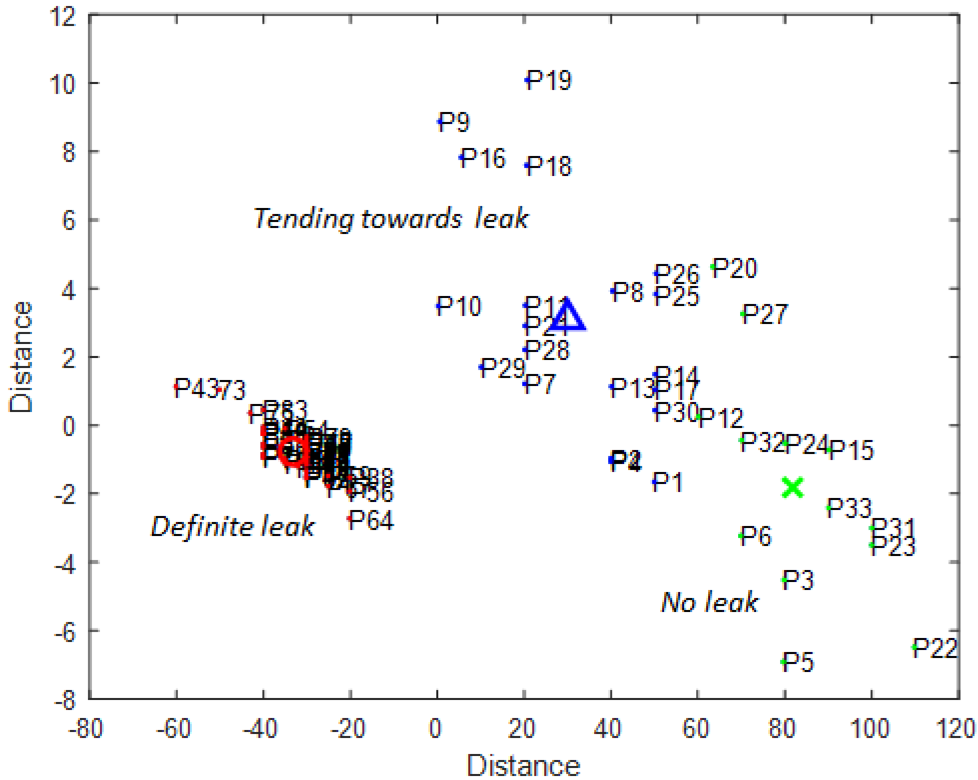

Figure 11: Fuzzy cluster distances between definite leak, tending towards a leak and no leak of from the discrepancy in data anomaly for voltage (x-axis) and amplitude (y-axis) for 3 centroids.

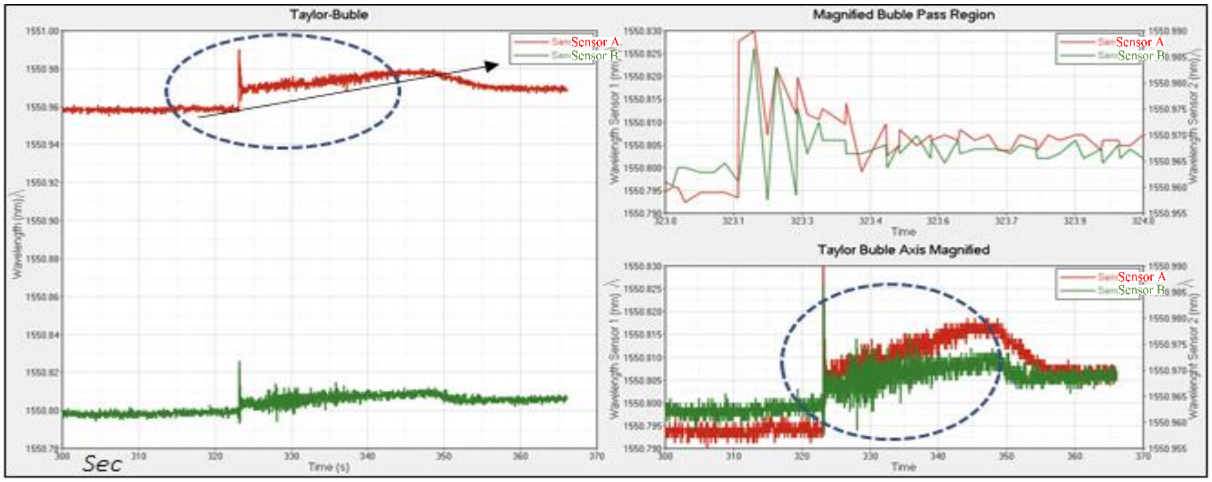

Figure 12: Associated trend line for passing of Taylor Bubble captured through Optical sensing indicating the shift and increased wavelength of such phenomenon. (highlighted in Red: bottom sensor, Green: top sensor).

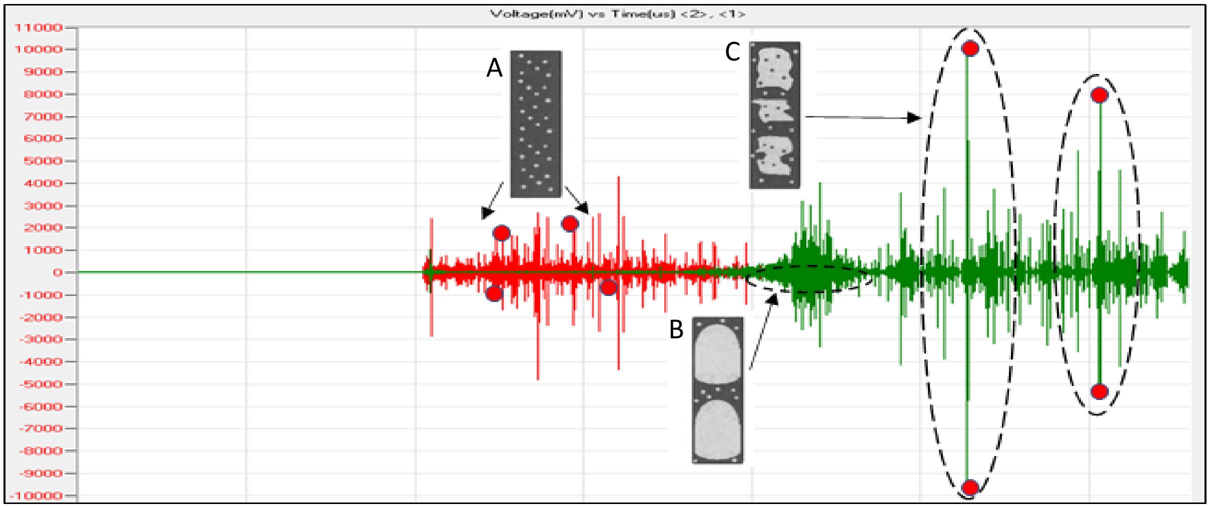

Figure 13: The magnified spectrum associated to the flow patterns in regard to AE sensing. From left to right: bubble flow, slug and slug-annular transition (Husin and Addali, 2010) (highlighted in Red: bottom sensor, Green: top sensor).